Journal of Power Sources 267 (2014) 260–268

Contents lists available at ScienceDirect

Journal of Power Sources

journal homepage: www.elsevier.com/locate/jpowsour

Welding of Nafion® – The influence of time, temperature and pressure

Konstantin Froelich [a, b, *], Helmut Rauner [a], Frieder Scheiba [b], Christina Roth [c], Helmut Ehrenberg [b]

[a] Produktions- und Werkstofftechnik (PWT), Daimler AG, Stuttgart, Germany
[b] Institute for Applied Materials – Energy Storage Systems (IAM-ESS), Karlsruhe Institute of Technology (KIT), Karlsruhe, Germany
[c] Institute of Chemistry and Biochemistry, Freie Universität Berlin, Berlin, Germany

HIGHLIGHTS

- We investigate the welding behavior of Nafion over a broad parameter range.
- The influence of time, temperature and pressure is measured and explained by theory.
- The welding behavior can be predicted by the reptation model from polymer dynamics.
- Time-temperature master curves for different pressures are constructed and discussed.
- Welding time and final strength are predicted using the model and measurement data.

ARTICLE INFO

Article history:
Received 15 February 2014
Received in revised form
30 April 2014
Accepted 7 May 2014
Available online 20 May 2014

Keywords:
Nafion®
Welding
Reptation model
Arrhenius temperature dependence
Pressure effect
Crystallinity

ABSTRACT

The properties of perfluorosulfonic acid ionomers (PFSIs) such as DuPont's Nafion® have been extensively characterized during the last decades. However, despite its importance for the upcoming industrialization of PFSI-based products no detailed investigation of the welding behavior of PFSIs has been performed. This paper investigates the welding behavior of Nafion® NRE-211 membranes common in both academia and industry over an industrially relevant parameter range of time, temperature and pressure. The strength evolution of the welded interface shows a linear dependence with square root of time and an Arrhenius temperature dependence. It is thus suggested that the welding behavior of Nafion® membranes can be predicted by the reptation model from polymer dynamics. Time-temperature master curves for a large range of parameters are constructed. Pressure is shown to have positive effects at very low welding times, but strongly negative effects at longer welding times, which can be explained by the model. Welding time and final strength of the fully healed interface are predicted using measurement and literature data. A short discussion on thermal transitions and on the role of crystallinity is also presented.

1. Introduction

Since the introduction of Nafion® by DuPont™ in the mid-1960s [1] perfluorosulfonic acid ionomers (PFSIs) have been extensively investigated for use as ion-conducting electrolyte in electrolysis cells, fuel cells and redox flow batteries as well as for different catalytic processes [2].

The hydrophobic Polytetrafluoroethylene (PTFE) backbone combined with the hydrophilic side chains result in the unique microstructural, thermomechanical and functional properties of PFSIs which despite thousands of publications have still not been fully understood [3]. One key characteristic of a PFSI molecule is the average distance between the hydrophilic side chains, characterized by the equivalent weight (EW) as molecular weight per mole of sulfonic acid groups. A typical equivalent weight of 1100 g mol^{-1} thus corresponds to an average of 6.6 TFE units between the side chains. The second distinct molecular feature of a PFSI molecule, the chemical structure and length of its side chain, has recently attracted increasing attention [4,5]. In contrast, the third molecular property, the molecular weight and its distribution, has received much less scientific attention. These molecular features as well as processing parameters and a slow equilibration to environmental conditions determine the microstructure and the resulting properties of PFSIs.

* Corresponding author. Produktions- und Werkstofftechnik (PWT), Daimler AG, Stuttgart, Germany. Tel.: +49 1781602539.
E-mail address: konstantin.froelich@daimler.com (K. Froelich).

http://dx.doi.org/10.1016/j.jpowsour.2014.05.026
0378-7753/

Today's understanding of the microstructure of PFSIs has mainly evolved from scattering and diffraction investigations performed since the 1970s. In an early investigation of Nafion® in its acid and precursor form Gierke et al. discovered that PFSIs have low crystallinity that can be assigned to the PTFE backbone, increases with increasing equivalent weight and decreases from the precursor to dry acid and wet acid form. Moreover, water filled clusters of around 5 nm size are detected, which increase in size and number along with an increased macroscopic water uptake with decreasing equivalent weight. It is further proposed that with increasing water content the number of side chains and average size per cluster increases, but the number of clusters is reduced by a microstructural reorganization [6]. Though a wealth of excellent investigations and microstructural models have been published thereafter (e.g. Refs. [7–20]) these assumptions from 1981 are still the foundations of our current understanding.

Thermomechanical properties have also been widely investigated towards a better understanding of PFSIs. In 1977, Yeo and Eisenberg identified three distinct thermal transitions of 1365 EW Nafion® at 110 °C, 20 °C and −100 °C, which they denoted by alpha, beta and gamma transition, which is still the current terminology [3,21]. Since then, dynamic mechanical analysis (DMA) [13,18–22], differential scanning calorimetry (DSC) [10,11,12,18,23], modulated differential scanning calorimetry (MDSC) [24], thermogravimetric analysis (TGA) [12,23], dielectric spectroscopy [20,21] as well as wide-angle X-ray diffraction (WAXD) [6], small-angle X-ray scattering (SAXS) [18,19] and nuclear magnetic resonance (NMR) spectroscopy [18] at different temperatures have been used to detect and interpret thermal transitions in PFSIs with, however, often contradictory results. This can be explained by the use of different PFSIs, their long equilibration times, but also by experimental difficulties as the effects of concurrent solvent evaporation during heating. The consensus is that the different transitions can be assigned to different molecular origins as a common glass transition of the backbone, a melting of the crystalline regions, the overcoming of electrostatic interactions between the side chain end groups and, finally, the thermal decomposition of PFSIs that starts at around 300 °C.

During the last decade the dependence of mechanical properties on environmental conditions as temperature and humidity has been further explored. Benzinger et al. find a drastic effect on Young's modulus, creep and relaxation rates [25–29]. Whereas water seems to have a plasticizing effect at temperatures below 70 °C, the hydrophilic clusters seem to have a stiffening effect at temperatures between 70 °C and 100 °C, which is supported by earlier results [22]. Recently, Patankar et al. showed that stress relaxation curves of PFSIs can be represented by master curves using time-temperature moisture superposition for a wide range of temperatures and humidities [30]. The same seems to apply to the fracture toughness of PFSI membranes characterized by a knife slit test [31,32].

Despite its importance for the upcoming industrialization of PFSI-based products the welding behavior of PFSIs has not been reported in detail before. In fact, it is sometimes suggested that welding of PFSI-based products should be conducted slightly above the glass temperature of a PFSI as a lower temperature could lead to insufficient melting [33] or a lack of molecular entanglements between the bond partners [34] and higher temperatures could lead to inferior product characteristics [33,34]. A detailed discussion of the underlying processes and resulting time temperature pressure trade-offs is lacking, however.

Polymeric parts can be bonded by a variety of joining technologies [35,36]. In contrast, PFSI-based parts such as membranes and electrodes for electrolysis cells, fuel cells or redox flow batteries require intimate contact between the bond partners, which is why welding seems to be the only appropriate joining technology. In welding, coalescence of the bond partners is typically reached by applying pressure and heat to the interface and the process is classified with respect to the heat source as thermal, friction or electromagnetic bonding [35]. In general, adhesion at the interface of two joined parts can be explained by a variety of possible adhesion models such as the thermodynamic adhesion model based on non-covalent bonds, the chemical adhesion model based on chemical bonds, the electrical adhesion model that interprets the two interfaces as a kind of capacitor, the diffusion model that is based on interdiffusion of matter across the interface and the mechanical adhesion model that is based on mechanical interlocking of the two bond partners and is probably the historically first explanation for adhesion. For polymers, it is now widely accepted that diffusion is the predominant adhesion mechanism in most cases [37–39].

From the basic idea of this adhesion mechanism presented by Voyutskii in the 1960s [40] today's models of polymer diffusion across an interface have evolved by a number of major works on polymer dynamics. Based on the work of Rouse on polymer dynamics in dilute solutions and melts [41], de Gennes [42], Doi and Edwards [43] also integrated the effects of molecular entanglements on chain dynamics and developed the "reptation model". According to the model thermal motion of linear polymer chains in an amorphous material can be described as a correlated, curvilinear motion of monomers within local restrictions imposed by neighboring chains or distant chain segments called "tubes". Starting with the chain ends, the chains leave their original tube by this random walk over time. After the molecular relaxation or reptation time T_r most of the chain has left its original tube. This model has first been applied to polymer interfaces by de Gennes, Prager and Tirell as well as Wool [38]. The latter characterizes the state of interdiffusion by several parameters such as the average length $l(t)$ of the chain ends that have left their original tube called "minor chains" resulting in the number of molecules $n(t)$ and the number of chain segments $p(t)$ crossing the interface. For a time $t < T_r$ these are defined as [38]

$$l(t) \approx 2\sqrt{(D_1 t/\pi)} = L\Big/2^{*}(t/T_r)^{0.5\sim}t^{0.5}M^{-0.5} \tag{1}$$

$$n(t) = \mathrm{n}_\infty{}^{*}(t/T_r)^{0.25\sim}t^{0.25}M^{-1.25} \text{ with } n_\infty = 1,31\rho\mathrm{N_a}(C_\infty j/M_0)b_0M^{-0.5\sim}M^{-0.5}. \tag{2}$$

$$p(t) = \mathrm{p}_\infty{}^{*}(t/T_r)^{0.5\sim}t^{0.5}M^{-1.5} \text{ with } p_\infty = 3,93\rho\mathrm{N_a}(C_\infty j/M_0)b_0M_c^{-0.5\sim}M^{0} \tag{3}$$

and

$$T_r \approx L^2\Big/(2D_1)^{\sim}M^3 \tag{4}$$

with D_1 as the curvilinear diffusion coefficient of a chain with length L, the density ρ, the molecular weight M, the molecular weight of the monomer M_0, the number of backbone bonds per monomer j, the characteristic ratio C_∞, the bond length b_0 and the Avogadro constant N_a. The temperature dependence of D_1 can be represented by an Arrhenius equation [44]. At times $t > T_r$ the chains have reached their equilibrium conformation and the interface has disappeared locally. The structure of the interface then only depends on molecular properties as seen in Eqs. (1)–(3). The mechanical strength of the interface is particularly dependent on the molecular weight, such that the mechanical strength starts at low values, then above a certain molecular weight increases by several orders of magnitude and levels off for further increasing

molecular weights. This threshold molecular weight called "critical molecular weight" is characteristic of the specific polymer. It is hypothesized that at the critical molecular weight the chains are sufficiently entangled or critically connected, which can be expressed as $p = 3 \times n$ with the above definitions.

The definitions above imply that at the time $t = 0$ the interfaces are in intimate physical contact. In contrast, real welding processes occur in several stages as microscopic wetting of the surfaces has to precede diffusion, which is why real welding processes have to be treated as a convolution of wetting and diffusion, as pointed out by Wool [45]. As wetting is a complex interplay of process parameters and properties of the parts to be welded it is often neglected or assumed to follow a linear dependence. The welding process of semicrystalline materials is further complicated as crystalline regions can evolve, grow or melt during wetting and diffusion. Alignment of molecules in crystalline sections obviously reduces the chain mobility, but crystallization can also break up the original interfaces by volume contraction [38]. Hence, the effects of crystallization can both improve or deteriorate the mechanical strength of the interface, again depending on both material and process parameters.

2. Experimental

To investigate the welding behavior of PFSI-based products, PFSI membranes were joined by hot-pressing with a heat sealing machine at different times, temperatures and pressures and the resulting seals were tested in a T-peel configuration with a regular tensile testing machine. As a reference membrane for both academia and industry with several publications on a variety of properties [30–32,46–49], DuPont™ Nafion® NRE-211 cast membranes were used for this study. All membranes were used as-received, which is closer to industrial use compared to the extensive pretreatment procedures often employed in scientific work. For sample preparation the membranes were cut with a roll-cutter to dimensions of 100 mm × 10 mm. The two protective foils called 'coversheet' and 'backing film' were then removed with adhesive tapes attached to a corner of the samples as proposed by DuPont™ [50]. The samples were cut in half and the two halves were carefully superimposed using teezers, such that the sides formerly facing the backing film were in contact, yielding a sample of 50 mm × 10 mm of two stacked membranes. Special attention was given to exactly align the two pieces as any overlap would lead to significant reduction in bonded area both impacting the welding pressure and the peel test evaluation. The actual welding process was performed at a Kopp Laboratory Sealer SGPE 3000 heat sealing machine using copper heat sealing bars with dimensions of 12.5 mm × 50 mm. Thus, an area of 12.5 mm × 10 mm was welded each time. To prevent the membrane samples from sticking to the heat sealing bars after welding, the samples were sheeted between temperature-resistant ETFE foils with a thickness of 100 μm and dimensions of around 30 mm × 70 mm. The sample stack now consisting of two membranes between ETFE foils was inserted between the heat sealing bars immediately before the welding process such that the foils did not touch the bars before the process. After welding, the samples were removed immediately from the heat sealing bars and left to cool on an aluminum plate. By a number of preliminary test runs it could be shown that the strength of the interface strongly increases, in case the samples are left between the heat sealing bars for any additional time before or after the actual welding process. The exact compliance with these described measures was thus imperative to yield good reproducibility. After cooling the ETFE foils were removed and the membrane samples were left to equilibrate around 10 min prior to testing. Standard adhesive tapes were attached to both unbounded peel arms to facilitate sample handling for the peel tests. For the peel tests a Zwick/Roell zwickiLineZ2.5 tensile tester with a 20 N load cell was used. The clamping length was set to 50 mm and a testing speed of 20 mm min^{-1} was selected. The sample configuration for the performed T-peel test as well as a typical load-displacement diagram resulting from the measurement are displayed in Fig. 1. As illustrated, two local maxima were typically encountered at the borders of the welded area. The height of these maxima proved to be dependent on time and temperature, but rather independent of pressure, whereas the ratio of local maxima to plateau-like curve strongly increased with pressure. With a number of samples stick-slip effects, a phenomenon related to rate-dependent fracture known for more than 25 years (e.g. Ref. [51]) with alternating jumping and very slow fracture propagation, could be observed at intermediate interfacial strengths.

To eliminate the boundary effects, the average peel force per peel width between around 20% and 80% of the displacement during fracture was taken as the representative value with a unit of N cm^{-1}. For T-peel tests this measured force per peel width does not correspond to the true fracture energy as often assumed for simplicity. In fact, a number of publications deal with this topic, additionally accounting for elastic and plastic effects in the peel arms in an energy balance (e.g. Ref. [52]). As a general consensus the true fracture energy is only a fraction of the overall energy measured in a peel test, which also depends on the properties of the material under investigation. Nevertheless, due to the complexity of this analysis and the large number of samples tested in this study, these approaches were not followed here. This

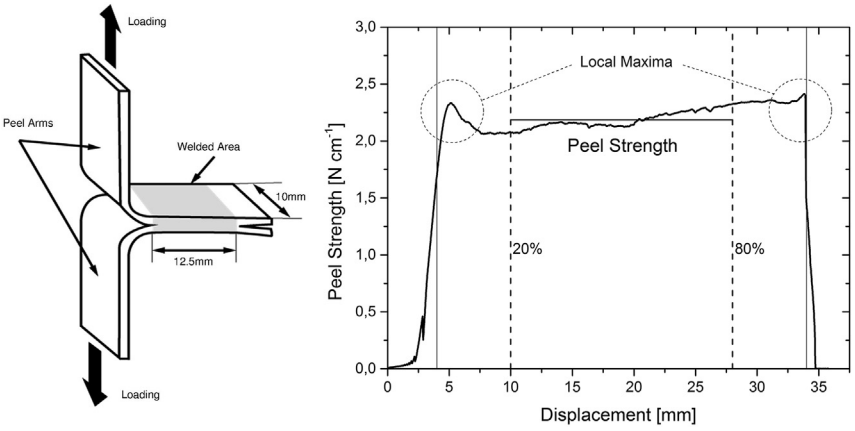

Fig. 1. Sample testing and data evaluation for the T-peel test applied.

assumes that true fracture energy and peel force per width or henceforth peel strength G_{IC} correlate in a proportional manner, which seems plausible considering that material and sample dimensions remain constant during this study.

In this study welding was performed with a broad range of industrially relevant parameters, with temperatures ranging from 120 °C to 200 °C, pressures from 0.4 MPa to 12 MPa and times from 0.3 s to 400 s. For each set of parameters 5 samples were prepared and tested yielding a total number of almost 400 samples. Mode III fracture of the welded areas (e.g. Ref. [53]), such that a crack propagated along the cross section of one of the membranes, resulted in the upper limit of peel strengths that could be measured, which is why the peel strength of fully healed interfaces could not be determined directly.

3. Results and discussion

The following section first discusses the influence of time and temperature at a low welding pressure of 0.4 MPa. The influence of pressure is investigated thereafter. This is followed by a short interpretation of the curve shape resulting in a theoretical prediction of the reptation time and the strength of the fully healed interface. A short discussion on thermal transitions and the role of crystallinity is presented as well.

3.1. The influence of time and temperature at low welding pressures

The influence of welding time and temperature on peel strength at a low welding pressure of 0.4 MPa is displayed in Fig. 2. As can be seen and is expected both time and temperature have a strong influence on the peel strength of the welded interface. Whereas at a temperature of 200 °C welding for 0.3 s results in a peel strength of around 1.5 N cm^{-1}, welding at 140 °C and 400 s only results in a peel strength of less than 1 N cm^{-1}. What is more interesting is that for a given temperature the influence of welding time on peel strength can be represented by a linear dependence on the square root of time over a large set of parameters as illustrated by the lines in Fig. 2. In fact, it exhibits the same time dependence as the average length of the minor chains $l(t)$ and the number of chain segments across the interface $p(t)$ predicted from the theoretical calculations of the reptation model given in Eqs. (1) and (3), respectively. However, these linear approximations do not run through the origin as would be expected if a linear correlation between $l(t)$ or $p(t)$ and peel strength existed. Thus, a more detailed examination appears necessary.

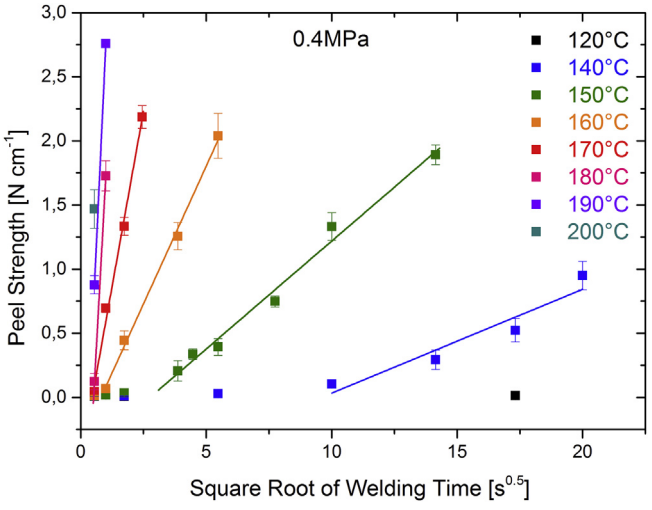

Fig. 2. Dependence of peel strength on time and temperature at a pressure of 0.4 MPa. The data points can be linearly approximated.

In case a correlation between mechanical strength and interfacial width exists [54] and if the interfacial width is well described by the reptation model, the linear sections of the graph should show an Arrhenius type temperature dependence. This further means that a time-temperature superposition can be deduced from the data.

In this case, the linear sections of the curve, i.e. the data for time t larger than the threshold time $t_{crit}(T)$, can be represented by the following equation with peel strength G_{Ic} for a set of parameters t and T, activation energy E_a, gas constant R and c_1, c_2 and c_3 as fitting parameters with c_1 and c_2 depending on temperature:

$$G_{Ic}(t,T) = c_1(T) + c_2(T)*t^{0.5} = c_1(T) + c_3*\exp(-E_a/(2RT))*t^{0.5} \text{ for } t > t_{crit}(T) \quad (5)$$

For the calculation of E_a all data with $G_{Ic}(t,T) > 0.05$ N cm^{-1} and with T between 140 °C and 190 °C were used, as these all seem to fit into a linear equation with $t^{0.5}$, which justifies this selection. Data fitting yields the values listed in Table 1. Fitting the logarithmic values of $c_2(T)$ with T in Kelvin then yields a fitting constant c_3 of $1.01*10^{16}$ N cm^{-1}s$^{-0.5}$ and a thermal activation energy E_a of 271 kJ mol^{-1}. For comparison, other authors mention thermal activation energies between 25 and 402 kJ mol^{-1} for polyethylene, polypropylene, polyisobutylene, poly(methyl methacrylate) (PMMA) and polystyrene (PS) [38,44]. For Nafion® NRE-211 membranes, thermal activation energies of 200 kJ mol^{-1} obtained by a knife slit test [32] and of 39 kJ mol^{-1} obtained from stress relaxation experiments [30] both in a temperature range from 40 to 100 °C are reported. Thus, the value of 271 kJ mol^{-1} deduced from our measurements seems to be a comparatively high, but reasonable value. As can be seen from Fig. 3 the data can be well represented by an Arrhenius dependence with only c_2(180 °C) and c_2(190 °C) deviating significantly from the fit, which will be further discussed later in the text.

A time-temperature superposition can now be constructed by using the following equation obtained using Eqs. (1) and (4) at two temperatures T_1 and T_2 with T_1 as temperature of the master curve

$$t_{T_2 \to T_1} = t*\exp((-E_a/R)*(1/T_1 - 1/T_2)) \quad (6)$$

Using the above equation a time-temperature superposition with respect to the reference temperature T = 140 °C can be constructed as shown in Fig. 4. Almost all data collapse well onto the master curve, with only some points deviating significantly. In fact, these are the values obtained for welding at 180 °C, 190 °C and 200 °C for 0.3 s as well as for 190 °C for 1 s, the latter two not illustrated for scaling reasons. These lower than predicted values can be explained, as for this extremely short welding time additional effects such as the wetting of the surfaces and, especially for higher temperatures, the heating of the interface could take a

Table 1
Data used for fitting of the linear sections and resulting threshold time t_{crit}.

Temperature [°C]	$c_1(T)$ [N cm^{-1}]	$c_2(T)$ [N cm^{-1} s$^{-0.5}$]	t_{crit} [s]	# samples in fit
140	−0.78	0.08	104.0	20
150	−0.47	0.17	9.3	30
160	−0.35	0.43	0.8	20
170	−0.50	1.09	0.3	18[a]
180	−1.82	3.55	0.3	10
190	−1.40	4.16	0.1	7[a]

[a] For the very high peel strengths for welding at 170 °C and 6 s and for 190 °C and 1 s only less than five valid measurements without mode III fracture could be obtained though a much bigger number of samples were tested.

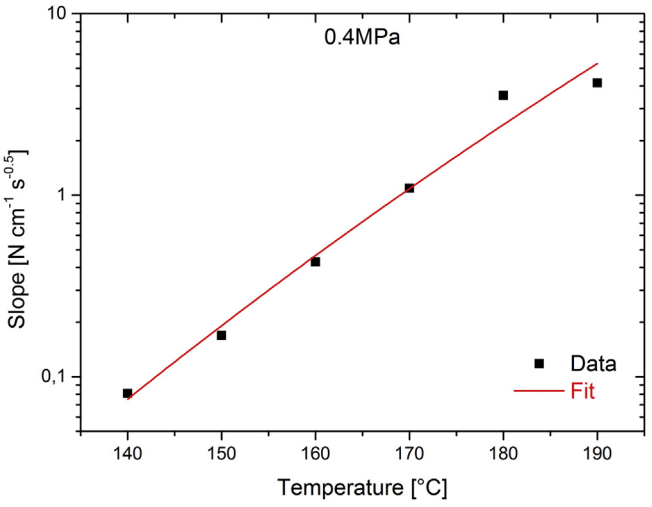

Fig. 3. Slope of the linear sections of peel strength versus time and temperature: data versus fit. Only at $T > 180$ °C the data and fit show significant deviation.

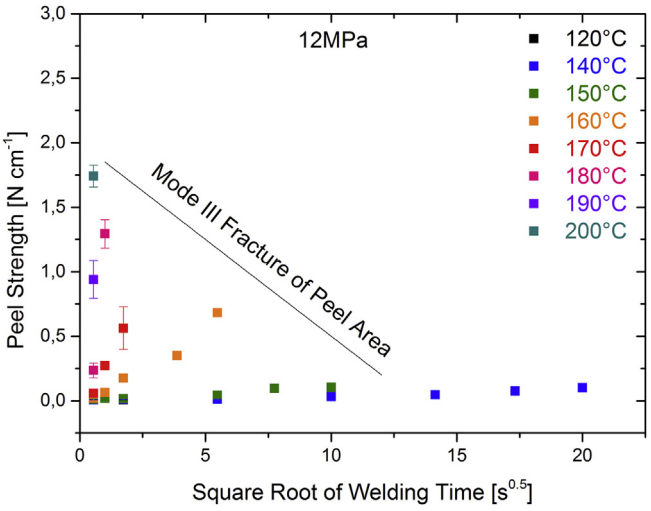

Fig. 5. Dependence of peel strength on time and temperature for 12 MPa. Pressure significantly reduces peel strength almost all data points.

significant amount of the total welding time. Thus, the welding behavior of NRE-211 membranes at low pressures can be represented by a time-temperature master curve for a wide range of industrially relevant parameters. Combined with the observed linear dependence of peel strength to the square root of time, this is a strong indication that the welding behavior of PFSIs can be well described and predicted by the reptation model for polymer diffusion. However, this prediction is complicated by the fact that there are two distinct sections in the master curve. Whereas during the first 100 s the peel strength slowly increases from around 0.08 N cm^{-1} to around 0.1 N cm^{-1}, the slope is much steeper in the linear section of the master curve. For practical purposes this means that a lot more data points have to be collected in order to retrieve the thermal activation energy and to predict the welding behavior. The origin of this distinct transition shall thus be discussed in Section 3.3 of this work.

3.2. The influence of welding pressure

Similar investigations were performed to evaluate the influence of pressure on welding. Apart from the previously discussed data obtained by welding at 0.4 MPa, further data were collected at 2.4 MPa and 12 MPa, respectively. The data obtained at pressures of 12 MPa are displayed in Fig. 5, which for better comparability uses the same scale as Fig. 2. Unwanted Mode III fracture of the samples occurred at similar time and temperature parameters compared to low pressure welding limiting the values which could be measured.

What can be seen immediately is the strongly negative effect of welding pressure on recorded peel strength for seemingly all data points, such that most data points are located below the transition to linear strength evolution. This could again be explained in the context of the reptation model, as the pressure is expected to reduce the chain mobility in an exponential manner [45]. Assuming the thermal activation energy is independent of pressure, the activation energy value obtained from the low pressure data was used to derive a time-temperature superposition for the 12 MPa data shown in Fig. 6.

As obvious from Fig. 6 the 12 MPa data do not collapse equally well onto a single time-temperature master curve as do the 0.4 MPa data. Taking a closer look it seems that the peel strengths for the 140 °C and 150 °C data mostly obtained at longer real welding times collapse onto a single curve. In contrast, the peel strengths for short welding times at 160 °C and 170 °C are significantly higher and do

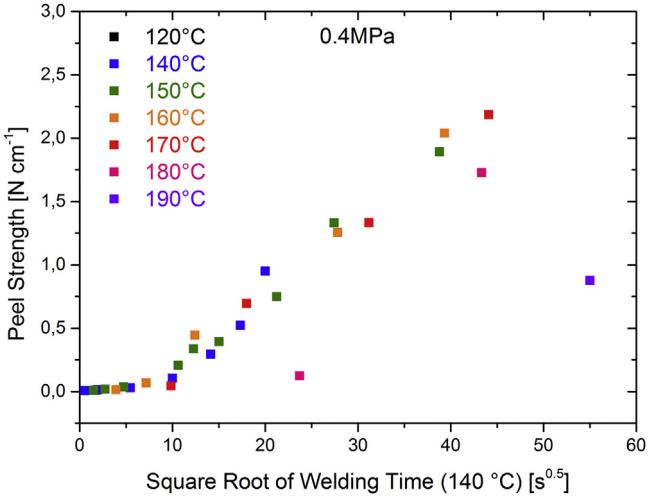

Fig. 4. Time-temperature master curve at 140 °C for low pressures. Almost all data collapse onto the master curve.

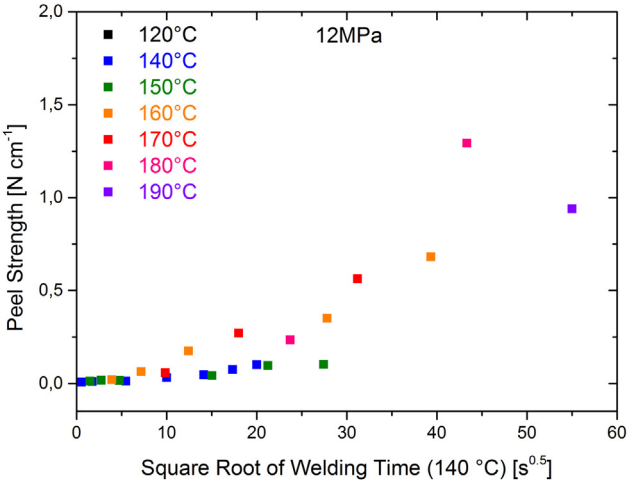

Fig. 6. Time-temperature master curve at 140 °C for high pressures. The high pressure data do not collapse equally well onto a master curve as the low pressure data do.

not seem to follow a clear trend. The peel strengths for longer welding times and for even higher temperatures seem to converge to a master curve again, but are still slightly higher than an extrapolation of the 140 °C and 150 °C data would imply. This suggests that especially for lower welding times an additional influence exists. To further analyze this effect the peel strengths obtained at 12 MPa and 0.4 MPa were compared by calculating the ratio G_{Ic}(12 MPa,t,T)/G_{Ic}(0.4 MPa,t,T) for different times and temperatures. These ratios as a function of time and temperature are shown in Fig. 7. As can be seen from the graph the ratio G_{Ic}(12 MPa,t,T)/G_{Ic}(0.4 MPa,t,T) displays a clearly decreasing trend with increasing welding time for all welding temperatures with the low pressure value being significantly higher as expected from the theory of diffusion. For very short welding times of 1 s and less, the opposite effect can be seen, such that increasing the pressure seems to have almost no effect or even a positive effect on the peel strength. This positive effect of pressure at very short welding time was verified by welding membranes at high speeds and temperatures in a calander, where higher pressures increased the peel strength up to a factor of 10. However, due to the limited set of data, these results shall not be further discussed at this point. It should further be mentioned that due to the change in slope of peel strength after a certain time t_{crit} as discussed above the data points in Fig. 7 should be interpreted only in a qualitative manner.

Nevertheless, these observations confirm the first interpretation of Fig. 6: In addition to the expected negative effect of pressure on diffusion pressure seems to have a positive effect at short welding times. Again, this can be well explained by the theory of polymer welding as a higher pressure can lead to faster wetting of the interfaces. Another possible explanation consistent with a positive effect of pressure at short welding times would be a faster temperature rise at the interface on account of a reduced thermal resistance at the interfaces between heat sealing bars, cover foil and NRE-211 membranes. For completeness, a possible misleading effect from a change in bulk properties of the welded areas of the membranes on the measured peel strengths has to be mentioned, but was shown to be negligible by applying the energy approach from Nase [52] on selected samples.

On account of this convolution of effects a meaningful time-temperature pressure superposition can only be performed for welding times higher than three seconds as the effects of interfacial heating and wetting disappear after this time. Instead, to better visualize the effects of pressure time-temperature master curves for different pressures are compared in Fig. 8. Again, the points for welding at 190 °C for 1 s and at 200 °C for 0.3 s are not included for scaling reasons. Nevertheless, as can be clearly seen, besides some scatter due to reasons discussed above a clearly negative effect of pressure can be seen for most data points. In fact, increasing the pressure from 0.4 MPa by a factor of 6 to 2.4 MPa seems to have a much lower effect than increasing the pressure from 2.4 MPa by a factor of 5 to a pressure of 12 MPa. This is again consistent with the theory of polymer dynamics that predicts an exponential influence of pressure on the curvilinear diffusion coefficient of a linear chain [45]. Finally, this is also consistent with the observation mentioned above that any dwell time of samples between the heat sealing bars before or after welding strongly increases peel strength of the interface meaning that welding is even possible with almost no pressure.

3.3. Welding time and final peel strength

Apart from the trade-offs between time, temperature and pressure extensively discussed above, welding time and the final strength of the fully healed interface are of critical interest for industrial applications. As previously mentioned, Mode III fracture of the bonded areas resulted in an upper limit of peel strengths that could be measured during this investigation, which is why welding time and final peel strength could not be directly deduced from the measurements. However, further information might be inferred by interpreting the transition between the two clearly distinguishable sections of peel strength versus time at threshold time t_{crit} previously defined. On the one hand, this transition could simply mean a change in the proportionality factor between measured peel strength and energy required to separate the welded interface. On the other hand, this transition could be owed to some kind of threshold at microscopic or molecular level. One interpretation could be that after time t_{crit} complete wetting of the interface has been reached such that unhindered diffusion can take place. While at first glance this seems plausible for high welding temperatures and resulting small values of t_{crit} (see Table 1), a deeper look discloses that the values of t_{crit} are not significantly reduced at a pressure of 12 MPa as compared to 0.4 MPa and that the transition seen for the 150 °C. 0.4 MPa data is sharper than implied by this interpretation. Furthermore, the effect of pressure proved to be positive only for welding times smaller than three seconds, whereas this transition occurred at much higher times for lower temperatures. Thus, this interpretation does not seem realistic. Another microscopic interpretation remains: As discussed above, molecular entanglements can drastically improve the mechanical strength of a polymer interface. The chains are said to be critically

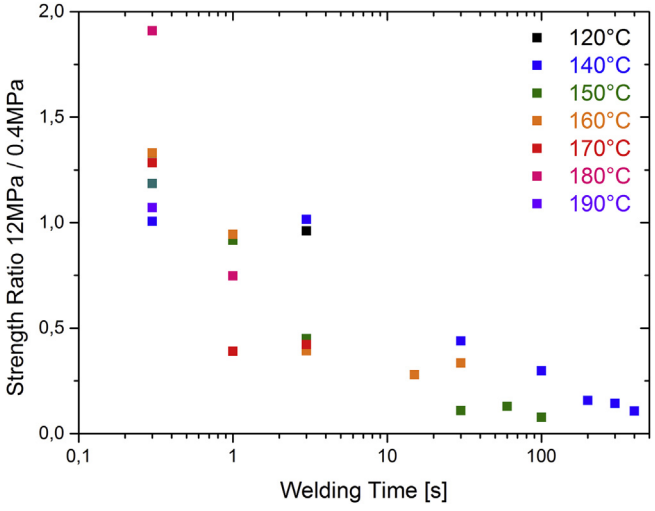

Fig. 7. Ratio of peel strengths at pressures of 12 MPa and 0.4 MPa.

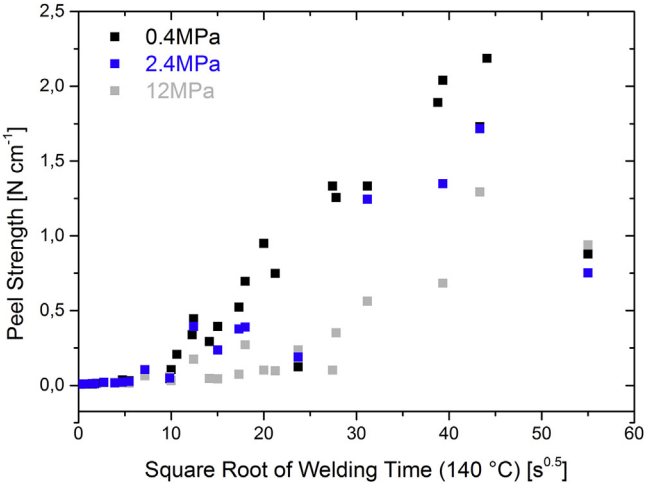

Fig. 8. Time–temperature master curves for different pressures.

connected if a certain threshold value of entanglements is reached such that bridges can be formed. In terms of the reptation model, this threshold value is reached if the number of chain segments p equals the number of chains n across the interface by at least a factor of three [38]:

$$p = 3{*}n \tag{7}$$

Inserting for p and n as defined in Eqs. (2) and (3) at time of critical connection t_{crit} yields:

$$\begin{aligned} p_\infty{*}(t_{crit}/T_r)^{0.5} &= 3{*}n_\infty{*}(t_{crit}/T_r)^{0.25} \Leftrightarrow (t_{crit}/T_r)^{0.25} \\ &= 3{*}(n_\infty/p_\infty) \Leftrightarrow t_{crit} = (M_c/M)^2{*}T_r \end{aligned} \tag{8}$$

According to that time t_{crit} only depends on the critical molecular weight M_c, the molecular weight M and the reptation time T_r defined in Eq. (1), which depends on the curvilinear diffusion coefficient D_1 that again follows an Arrhenius temperature dependance with activation energy E_a as calculated above. Hence, the observed transition time t_{crit} should follow an Arrhenius dependence with E_a = 271 kJ mol^{-1}. This goes along well with the experimental values for t_{crit} and temperatures up to 170 °C. At even higher temperatures the experimental t_{crit} is higher than predicted, which seems reasonable due to the additional effects of wetting and heating and experimental difficulties at welding times of 1 s and less. It is thus proposed that the observed transition in peel strength is attributable to the interface reaching a threshold number of entanglements to be critically connected. This means that the transition is due to molecular properties as opposed to macroscopic properties such as membrane thickness.

In case this is true, the reptation time can be predicted based on the experimental t_{crit} and information on the molecular weight M and critical molecular weight M_c of the investigated 1100 EW Nafion®. Unfortunately, only very limited data on molecular properties of PFSIs have been published, which can be explained by the fact that PFSIs hardly form true solutions. Whereas it is generally accepted that the molecular weight of Nafion® is between 10^5 Da and 10^6 Da [3], only very few publications with actual measurements of M exist [2,55–57]. Though PFSIs from different companies and with different EWs have been studied all studies report weight average molecular weights M_w between 2×10^5 Da and slightly above 3×10^5 Da with significant polydispersity. For the following calculation the 1100 EW Nafion® used in this study is assumed to have the same weight average molecular weight M_w as the 1000 EW Nafion® examined by DuPont with $2{,}5 \times 10^5$ Da [55]. No literature data on the critical molecular weight M_c are available, so that it will be estimated from the following approximate formula for vinyl polymers of infinite chain length [38] with C_∞ and M_0 as defined above:

$$M_c = 30{*}C_\infty{*}M_0 \tag{9}$$

Regarding the characteristic ratio again hardly any literature data on Nafion® exist. Whereas Wescott et al. [58] use a value of 7.13, Mourey et al. [57] experimentally determine values between 3.7 and 5.7 for different PFSIs. However, as Mourey et al. point out these values seem unrealistically small so that the value of 7.13 from Wescott et al. is used here. The molecular weight M_0 of the NRE-211 monomer finally is 1100 Da per definition, but has to be divided by the number of PTFE backbone units as the characteristic ratios from above refer to one PTFE unit as a monomer. Hence, a value of 1100/7.6 = 144.7 Da was used for M_0. Inserting into Eq. (9) this yields a critical molecular weight M_c of 30,959 Da. Rearranging Eq. (8) and using the experimental t_{crit} thus predicts reptation times between around 113 min at 140 °C and 16.4 s at 170 °C for 0.4 MPa. Of course, considering the above approximations this can only be used as a rough estimate, but nevertheless it underlines the crucial influence of temperature on welding of Nafion®. Strictly speaking, the reptation time T_r is only an upper bound for welding time as the final strength can be reached at lower times for polymers with very high molecular weights. Neglecting this potential influence and assuming the observed linear trend of peel strength with square root of time continues up to reptation time T_r the strength of the fully healed interface can be estimated by inserting the temperature dependent T_r values into Eq. (5). This yields a range of final peel strengths between 2.85 N cm^{-1} and 5.89 N cm^{-1} for temperatures between 140 °C and 170 °C. In fact, these predicted values are on the same order of magnitude as the highest experimental value of 2.76 N cm^{-1}, which supports this interpretation. Finally, this maximum peel strength might also explain why the slope of peel strength with square root of time $c_2(T)$ for 190 °C and 0.4 MPa is lower than expected (see Fig. 3): On account of the expected significant polydispersity some shorter chains have already reached their equilibrium state before the interface has fully healed, which is why the curve flattens.

So how do these measured and predicted peel strengths compare with literature data on the fracture strength of Nafion®? The highest measured value of 2.76 N cm^{-1} translates to a fracture energy of 276 J m^{-2}. The theoretical prediction presented above would yield values between 285 J m^{-2} and 589 J m^{-2}. With an energy approach on peeling as proposed by Nase et al. [52] these values would be significantly lower, but still of the same order of magnitude. For comparison, other researchers [31,32] determine NRE-211 fracture strengths of several kJ m^{-2} by trouser tear test and of 200 J m^{-2} to 1 kJ m^{-2} by knife slit test depending on testing temperature, humidity and speed. Considering that experimentally determined fracture strengths strongly depend on test method and parameters this is in good agreement with the measurements and predictions presented above.

3.4. Thermal transitions and the role of crystallinity

It might be worth to more generally interpret the welding data presented above, also with respect to supplemental measurements and literature data. Most important, no distinct thermal transition can be observed over the whole temperature range from 140 °C to 190 °C relevant for industrial processing. Instead, the data can be well represented by an Arrhenius temperature dependence. As no investigation on thermal transitions of NRE-211 are known to the author, data on 1100 EW Nafion® 112 from DuPont, which should have the same molecular structure, might serve as a reference. Recently, Zawodzinski et al. [24] applied MDSC on Nafion® 112. Apart from a broad non-reversing endothermic peak between 30 °C and 155 °C, which can be explained by volatilization of solvents contained in the membrane, an endothermic step change similar to a glass transition is observed between 100 °C and 200 °C and ascribed to the ionic clusters. To gain a reference for NRE-211 own DSC measurements were performed from 10 °C to 340 °C with 10 °C min^{-1} heating rate for 5 samples using sealed cups to suppress solvent volitilization in the temperature range of interest. Between 10 °C and 185 °C only one simple glass transition between 150 °C and 155 °C with a step size around 0.6 J g^{-1} °C^{-1} was observed. Between 185 °C and 220 °C a sharp endothermic peak with an area of around 100 J g^{-1}, attributed to solvent evaporation, then no further transition up to 340 °C could be detected.[1] These DSC measurements agree well with the data and interpretation from Zawodzinski et al. There seems to be a glass transition in 1100

[1] The peak around 200 °C seems quite sharp for an evaporation process. However, the peak goes along with a sudden buckling of the sealed cups, such that the volume increases fast, which could explain this observation.

EW Nafion® at around 150 °C. However, this bulk glass transition is not visible in the welding data. Nevertheless, this is no contradiction, as during the last 15 years many investigations have shown that chains at a polymer surface have a different conformation, energy state and mobility than the bulk phase, which leads to a surface glass temperature distinctly lower than the bulk glass temperature of the polymer [59–61]. Thus, NRE-211 seems to have a bulk glass temperature of around 153 °C and a surface glass temperature lower or equal to 140 °C.

Another point of interest is the existence and role of the crystalline sections. As discussed above PFSIs are semicrystalline with the crystalline content depending on the chemical structure and processing. The same is true for NRE-211 that seems to have a crystallinity of around 12% as calculated from the intensities of the fitted amorphous and fitted crystalline peak from WAXD measurements, which can be slightly increased by heat treatment [48]. Own preliminary WAXD measurements confirm the existence of crystalline sections. However, no peaks displaying melting of the crystalline sections could be observed in our DSC measurements. This might be explained by the observation in WAXD measurements at varying temperatures from Gierke et al. [6] that the crystalline sections in the precursor melt over a wide temperature from 50 °C to 270 °C. Still, crystallinity could play an important role in welding, as it strongly reduces the chain mobility. For example, the strongly negative effect of pressure on peel strength might also be explained by the Clapeyron effect for semicrystalline polymers mentioned by other researchers [62,63]. Melting of crystalline sections might also explain the higher activation energy E_a obtained from our welding data compared to the E_a values for knife slit fracture and stress relaxation of NRE-211 obtained by Patankar et al. for a range from 40 °C to 100 °C [30,32]. As all of these processes depend on polymer dynamics the respective E_a values should be the same, if no additional effects were involved.

4. Conclusions and outlook

For the first time, the welding behavior of PFSIs has been investigated in detail over an industrially relevant range of parameters using Nafion® NRE-211 membranes from DuPont™ as a representative product. It has been shown that the strength of the welded interface depends strongly on the process parameters time, temperature and pressure. The strength of the welded interface shows a linear dependence on square root of time above a temperature-dependent threshold time t_{crit} and an Arrhenius temperature dependence with thermal activation energy E_a of around 270 kJ mol^{-1}. Pressure can have positive effects at welding times of one second or less and has strongly negative effects at higher welding times, which can be explained by theory. It has further been shown that time-temperature superposition curves can be constructed for most of the parameter range. Only for high pressures combined with high temperatures and welding times of 3 s or less additional effects attributed to the convolution of heating, wetting and diffusion disturb the master curve. These observations strongly suggest that despite their complex morphology with ionic clustering and crystalline sections the welding behavior of PFSIs can be modeled and predicted by the reptation model for amorphous linear polymers over the whole industrially relevant parameter range.

Based on the assumption of polymer diffusion as the dominating mechanism, the transition to linear dependence of peel strength on square root of time at a threshold time t_{crit} was ascribed to the state of a critically connected network. Based on this assumption and the reptation model for polymer dynamics welding time and final peel strength of the fully healed interface were predicted using the measured t_{crit} as well as the molecular weight gained from the literature and the critical molecular weight estimated using an approximate formula from polymer theory. According to this prediction, increasing the welding temperature by only 30 °C from 140 °C to 170 °C reduces the time required for full interfacial healing from around 113 min to only 16.4 s. The predicted strength of the fully healed interface is in good agreement with the maximum measured values, but also with fracture data obtained by other researchers using different methods. Based on the welding data and supplementary DSC measurements a bulk glass temperature of 153 °C and a surface glass temperature lower or equal to 140 °C were determined for NRE-211 membranes. The role of crystallinity on welding was shortly discussed with the Clapeyron effect as possible alternative explanation for the strongly negative pressure effect, which should be further investigated.

On a longer perspective, the importance of molecular weight and related properties of PFSIs has been highlighted. Apart from the recently predicted influence on morphology [64], molecular weight strongly influences strength development and required time for welding of PFSI-based products. Finally, the present investigation displays the importance of a polymer dynamics approach for processing of PFSI-based products.

References

[1] D.J. Conolly, W.F. Gresham, Fluorocarbon Vinyl Ether Polymers, US Patent 3282875, 1966.
[2] D. Curtin, R. Lousenberg, T. Henry, P. Tangemann, M. Tisack, J. Power Sources 131 (2004) 41–48.
[3] K. Mauritz, R. Moore, Chem. Rev. 104 (2004) 4535–4585.
[4] A. Ghielmi, P. Vaccarono, C. Troglia, V. Arcella, J. Power Sources 145 (2005) 108–115.
[5] K.D. Kreuer, M. Schuster, B. Obliers, O. Diat, U. Traub, A. Fuchs, U. Klock, S.J. Paddison, J. Maier, J. Power Sources 178 (2008) 499–509.
[6] T.D. Gierke, G.E. Munn, F.C. Wilson, J. Polymer Sci. Polym. Phys. Ed. 19 (1981) 1687–1704.
[7] M. Fujimura, T. Hashimoto, H. Kawai, Macromolecules 14 (1981) 1309–1315.
[8] H.L. Yeager, A. Steck, J. Electrochem. Soc. 128 (1981) 1880–1884.
[9] G. Gebel, P. Aldebert, M. Pineri, Macromolecules 20 (1987) 1425–1428.
[10] R.B. Moore, C.R. Martin, Macromolecules 21 (1988) 1334–1339.
[11] R.B. Moore, C.R. Martin, Macromolecules 22 (1989) 3594–3599.
[12] I.D. Stefanithis, K.A. Mauritz, Macromolecules 23 (1990) 2397–2402.
[13] R.B. Moore, K.M. Cable, T.L. Croley, J. Membr. Sci. 75 (1992) 7–14.
[14] G. Gebel, P. Aldebert, M. Pineri, Polymer 34 (1993) 333–339.
[15] G. Gebel, Polymer 41 (2000) 5829–5838.
[16] P.C. van der Heijden, L. Rubatat, O. Diat, Macromolecules 37 (2004) 5327–5336.
[17] G. Gebel, O. Diat, Fuel Cells 5 (2005) 261–276.
[18] K.A. Page, K.M. Cable, R.B. Moore, Macromolecules 38 (2005) 6472–6484.
[19] K.A. Page, F.A. Landis, A.K. Phillips, R.B. Moore, Macromolecules 39 (2006) 3939–3946.
[20] S.J. Osborn, M.K. Hassan, G.M. Divoux, D.W. Rhoades, K.A. Mauritz, R.B. Moore, Macromolecules 40 (2007) 3886–3890.
[21] S.C. Yeo, A. Eisenberg, J. Appl. Polym. Sci. 21 (1977) 875–898.
[22] F. Bauer, S. Denneler, M. Willert-Porada, J. Polym. Sci. B Polym. Phys. 43 (2005) 786–795.
[23] S.H. de Almeida, Y. Kawano, J. Therm. Anal. Calorim. 58 (1999) 569–577.
[24] C.N. Sun, K.L. Moore, T.A. Zawodzinski, ECS Trans. 33 (2010) 1207–1215.
[25] M.B. Satterfield, Dissertation, Princeton University, 2007.
[26] P.W. Majsztrik, A.B. Bocarsley, J.B. Benzinger, Macromolecules 41 (2008) 9849–9862.
[27] P.W. Majsztrik, Dissertation, Princeton University, 2008.
[28] M.B. Satterfield, J.B. Benzinger, J. Polym. Sci. B Polym. Phys. 47 (2009) 11–24.
[29] A. Bocarsley, D.M. Mingos (Eds.), Fuel Cells and Hydrogen Storage, Springer, Berlin, 2011, pp. 85–113.
[30] K.A. Patankar, D.A. Dillard, S.W. Case, M.W. Ellis, Y.H. Lai, C.S. Gittleman, Fuel Cells 12 (2012) 787–799.
[31] J. Li, J.K. Quincy, S.W. Case, M.W. Ellis, D.A. Dillard, Y.-H. Lai, M.K. Budinski, C.S. Gittleman, J. Power Sources 185 (2008) 374–380.
[32] K.A. Patankar, D.A. Dillard, S.W. Case, M.W. Ellis, Y. Li, Y.-H. Lai, M.K. Budinski, C.S. Gittleman, J. Polym. Sci. B Polym. Phys. 48 (2010) 333–343.
[33] J. Zhang (Ed.), PEM Fuel Cell Electrocatalysts and Catalyst Layers – Fundamentals and Applications, Springer-Verlag London Limited, London, 2008, pp. 889–916.
[34] H.-Y. Jung, J.W. Kim, Int. J. Hydrogen Energy 37 (2012) 12580–12585.
[35] V.K. Stokes, Polym. Eng. Sci. 29 (1989) 1310–1324.
[36] R.P. Wool, B.-L. Yuan, O.J. McGarel, Polym. Eng. Sci. 29 (1989) 1340–1367.
[37] H.R. Brown, Annu. Rev. Mater. Sci. 21 (1991) 463–489.

[38] R.P. Wool, Polymer Interfaces: Structure and Strength, first ed., Hanser Publishers, Munich, 1995.
[39] G. Fourche, Polym. Eng. Sci. 35 (1995) 957–967.
[40] S.S. Voyutskii, Autohesion and Adhesion of High Polymers, first ed., Interscience Publishers, New York, 1963.
[41] P.E. Rouse, J. Chem. Phys. 21 (1953) 1272–1280.
[42] P.-G. de Gennes, J. Chem. Phys. 55 (1971) 572–579.
[43] M. Doi, S.F. Edwards, J. Chem. Soc. Faraday Trans. 2 Mol. Chem. Phys. 74 (1978) 1789–1801.
[44] K. Jud, H.H. Kausch, J.G. Williams, J. Mater. Sci. 16 (1981) 2014–2210.
[45] R.P. Wool, M.K. O'Connor, Polym. Eng. Sci. 21 (1981) 970–977.
[46] M. Adachi, T. Navessin, Z. Xie, B. Frisken, S. Holdcroft, J. Electrochem. Soc. 156 (2009) B782–B790.
[47] J. Peron, A. Mani, X. Zhao, D. Edwards, M. Adachi, T. Soboleva, Z. Shi, Z. Xie, T. Navessin, S. Holdcroft, J. Membr. Sci. 356 (2010) 44–51.
[48] J. Li, X. Yang, H. Tang, M. Pan, J. Membr. Sci. 361 (2010) 38–42.
[49] R. Jia, B. Han, K. Levi, T. Hasegawa, J. Ye, R.H. Dauskhardt, J. Power Sources 196 (2011) 3803–3809.
[50] DuPont™, Datasheet Nafion® PFSA Membranes, NRE-211 and NRE-212.
[51] J.W. Gillespie, L.A. Carlsson, A.J. Smiley, Compos. Sci. Technol. 28 (1987) 1–15.
[52] M. Nase, B. Langer, W. Grellmann, Polym. Test. 27 (2008) 1017–1025.
[53] T.L. Anderson, Fracture Mechanics: Fundamentals and Applications, first ed., CRC Press, Boca Raton, 2005.
[54] R. Schnell, M. Stamm, C. Creton, Macromolecules 31 (1998) 2284–2292.
[55] R.D. Lousenberg, J. Polym. Sci. B Polym. Phys. 43 (2005) 421–428.
[56] W.-H. Liu, T.-Y. Yu, T.L. Yu, H.-L. Li, e-Polymers 109 (2007) 1–8.
[57] T.H. Mourey, L.A. Slater, R.C. Galipo, R.J. Koestner, J. Chromatogr. A 1218 (2011) 5801–5809.
[58] J.T. Wescott, Y. Qi, L. Subramanian, T.W. Capehart, J. Chem. Phys. 124 (2006) 134702:1–134702:14.
[59] Y.M. Boiko, R.E. Prud'homme, Mech. Compos. Mater. 35 (1999) 441–446.
[60] Y.M. Boiko, G. Guérin, V.A. Marikhin, R.E. Prud'homme, Polymer 42 (2001) 8695–8702.
[61] Y.M. Boiko, J. Polym. Sci. B Polym. Phys. 48 (2010) 2012–2021.
[62] S.B. Warner, Text. Res. J. 59 (1989) 151–159.
[63] S. Michielson, B. Pourdeyhimi, P. Desai, J. Appl. Polym. Sci. 99 (2006) 2489–2496.
[64] D. Wu, S.J. Paddinson, J.A. Elliott, Macromolecules 42 (2009) 3358–3367.